# Rapid Thermal Annealing Effects on Passivation Quality of p-TOPCon Silicon Solar Cells

Arpan Sinha, *Member, IEEE*, Sagnik Dasgupta, *Graduate Student Member, IEEE*, Ajeet Rohatgi, *Life Fellow, IEEE*, and Mool C. Gupta, *Fellow, IEEE* 

Abstract—Unlike the traditional tube-furnace annealing at 875 °C, rapid thermal annealing (RTA) and laser annealing offer flexibility, high throughput, and control of the heating and cooling rates and holding times for effective crystallization, dopant activation, and passivation quality in the B-doped p-TOPCon device. A comprehensive scientific understanding of the effects of RTA is required. Slower RTA heating ( $\leq$  798 K/min) and cooling ( $\leq$  156 K/min) rates and optimal 60 s holding time at 825 °C enhanced the passivation quality, which was further improved by postanneal forming gas annealing (FGA). Faster heating and cooling rates ( $\geq$  4800 K/min) damaged the passivation quality irreversibly and did not improve further by FGA. The optimized RTA parameters yielded  $iV_{\rm oc}$  of 638 mV and sheet resistance of  $\sim$ 1.0 kΩ/sq. The dopant activation was independent of the heating and cooling rates.

*Index Terms*—Boron, cooling, heating, holding, p-tunnel oxide passivated contacts (TOPcon), rapid thermal annealing (RTA), silicon solar cells.

### I. INTRODUCTION

HE tunnel oxide passivated contacts (TOPCon) Si solar cell, one of the most competitive c-Si solar cell architectures, is known for its simple architecture, easy fabrication, high thermal stability, and resilience to postmetallization annealing. The state-of-the-art lab-based efficiencies of n-TOPCon (based on n-type Si wafer) and p-TOPCon (based on p-type Si wafer) solar cells are 25.8% and 26.1%, respectively [1], [2]. The TOPCon c-Si architecture comprises stack layers of ultrathin ( $\sim$ 1.5 nm) SiO<sub>x</sub>, highly doped polycrystalline Si (poly-Si), and an optional SiN<sub>x</sub>:H or SiC<sub>x</sub>:H coating.

One of the essential steps in the fabrication of TOPCon solar cells is thermal annealing, which is necessary for dopant activation, crystallization, lower c-Si/SiO $_{\rm x}$  interfacial defects, and lower sheet resistance. Generally, annealing is performed at high temperatures (800–900 °C) using the traditional tube-furnace anneal and conveyor belt-furnace anneal under an inert

Manuscript received 16 October 2023; revised 27 November 2023; accepted 20 December 2023. Date of publication 15 January 2024; date of current version 20 February 2024. This work was supported by National Science Foundation under Grant ECCS-2005098 and Grant I/UCRC-1338917. (Corresponding author: Mool C. Gupta.)

Arpan Sinha and Mool C. Gupta are with the Department of Electrical and Computer Engineering, University of Virginia, Charlottesville, VA 22904 USA (e-mail: as2ag@virginia.edu; mgupta@virginia.edu).

Sagnik Dasgupta and Ajeet Rohatgi are with the Department of Electrical and Computer Engineering, Georgia Institute of Technology, Atlanta, GA 30332 USA (e-mail: sdasgupta@gatech.edu; ajeet.rohatgi@ece.gatech.edu).

Color versions of one or more figures in this article are available at https://doi.org/10.1109/JPHOTOV.2023.3348239.

Digital Object Identifier 10.1109/JPHOTOV.2023.3348239

atmosphere, such as  $N_2$  [3], [4], [5], [6]. The disadvantages of furnace annealing are an enormous thermal budget, longer annealing time, less flexibility, and lower throughput.

Due to its several advantages, such as the choices of annealing atmosphere, better control of the annealing durations (from a few seconds to several minutes), and flexible ramping rates of heating and cooling, rapid thermal annealing (RTA) has emerged as an alternative cost-effective, high-yield processing tool for dopant activation and crystallization [7], [8]. Moreover, the RTA has been used to perform forming gas annealing (FGA) for external hydrogenation. In our recent publication, we have shown the RTA and FGA applications to achieve high implied open-circuit voltage ( $iV_{oc}$ ) of 706 mV through crystallization and high dopant activation in B-doped p-TOPCon c-Si solar cells with SiN<sub>x</sub>:H capping layer [9]. Yang et al. [8] reported the fabrication of 23.04% efficient Al<sub>2</sub>O<sub>3</sub>-capped P-doped n-TOPCon c-Si solar cells with  $iV_{\rm oc}$  as high as 727 mV by RTA treatment. Similar studies are needed for p-TOPCon c-Si solar cells. Since RTA shows such promising results, it is crucial to understand the physics behind the thermal cycle dynamics and achieve results equivalent to the traditional furnace annealing for p-TOPCon c-Si solar cells. It will also help understand and optimize fast laser processing for p-TOPCon c-Si fabrication since laser processing involves fast heating and cooling rates [10].

The highly B-doped poly-Si layer on top of the ultrathin  $\mathrm{SiO}_x$  layer provides additional field-effect passivation, provided that the thickness of  $\mathrm{SiO}_x$  is < 1.6 nm. At annealing temperatures < 850 °C, the charge carrier transport occurs through the quantum tunneling effect as pinhole formation is minimal. At temperatures beyond 850 °C, more pinholes form, and charge conduction through pinholes dominates the tunneling mechanism. The pinholes created in the  $\mathrm{SiO}_x$  layer act as a gateway for the B-dopant to diffuse into the bulk Si. This diffused layer further enhances the electrical field to maximize the field-effect passivation. On the other hand, excess dopant diffusion into the bulk Si causes more considerable Auger recombination, which cannot be compensated by the enhanced field-effect passivation and leads to passivation degradation [11], [12].

Yang et al. [13] recently reported the heating and cooling effects on TOPCon structures using quartz tube-furnace annealing. As the annealing temperature increases during heating, poly-Si, ultrathin  $\mathrm{SiO}_{\mathrm{x}}$ , and c-Si substrates expand. Due to higher thermal expansion coefficients, c-Si and poly-Si expand more than ultrathin  $\mathrm{SiO}_{\mathrm{x}}$ , which produces compressive stress in the substrate and tensile stress in the ultrathin  $\mathrm{SiO}_{\mathrm{x}}$ . This tensile

2156-3381 © 2024 IEEE. Personal use is permitted, but republication/redistribution requires IEEE permission. See https://www.ieee.org/publications/rights/index.html for more information.

stress grows faster, causing concave distortion and fracture in the  $SiO_x$ , forming pinholes to relieve the accumulated tensions. On the contrary, cooling induces more inward shrinkage of both c-Si and poly-Si than ultrathin  $SiO_x$ , causing tensile stress in the substrate and compressive stress in the  $SiO_x$ , eventually increasing pinholes.

Although this pinhole mechanism finding provides a good understanding of tube-furnace annealing effects, understanding of RTA effects is still lacking as the overall heating, holding, and cooling methodologies differ. So, there is a need to understand the effects of RTA heating and cooling rates and holding time on the surface passivation quality, dopant activation, crystallization, and defect states in B-doped poly-Si-based p-TOPCon devices. Previously, Hollemann et al. [14], [15] showed that significant temperature gradients increase mechanical stresses and the density of defect states at the SiO<sub>x</sub>/c-Si interface during tube-furnace annealing of P-doped poly-Si-based n-TOPCon devices. Earlier reports also stated that cooling times influence the severity of thermal stress more than heating times [16]. Moreover, similar findings on the effects of slower RTA cooling rates on the minority carrier lifetime and defect densities were demonstrated in the fabrication of n<sup>+</sup>-p-p<sup>+</sup> Si and p-type mc-Si devices. Still, the optimization of heating rates and holding times remained unexplored [17], [18], [19]. It has also been suggested that the high radial-temperature nonuniformity in Si substrates causes stresses beyond its yield point due to the one-sided heating in the RTA system [20]. Earlier, Yang et al. [8] described the optimization of longer RTA holding and cooling times of n-TOPCon devices, and Shou et al. [21] used similar optimization for annealing their TOPCon devices. However, their findings were limited to PECVD P-doped n-TOPCon devices with a total RTA processing duration of  $\sim$ 27 min (similar to the traditional tube-furnace annealing durations), and the effects of heating times were not discussed.

Hence, in this article, we investigated the effects of RTA heating and cooling rates as well as holding time on the passivation quality,  $iV_{\rm oc}$ , and dopant activation of *in situ* B-doped poly-Si-based p-TOPCon Si solar cells. The potential of using RTA for fast processing was also evaluated for high throughput. Device characterizations were conducted using photoluminescence (PL), quasi-steady-state photoconductance (QSSPC), and four-point probing to better understand the RTA processing.

### II. EXPERIMENT

The p-TOPCon architecture involves an *in situ* B-doped poly-Si/SiO<sub>x</sub> stack on n-type c-Si wafers. This approach offers advantages over *ex situ* boron doping, including simplicity, independence from dopant predeposition, higher throughput, elevated poly-Si deposition rate, increased boron concentration, enhanced field-induced passivation, and reduced optimal annealing temperature. Fig. 1 illustrates the schematic diagram of the TOPCon test structure. These structures were fabricated on 200  $\mu$ m thick n-type monocrystalline Cz-type <100> silicon wafers featuring a bulk resistivity of 3.2  $\Omega$ ·cm. After removing the saw damage in 9% wt. KOH at 80 °C for 12 min, the surface was semiplanarized. The wafers underwent cleaning

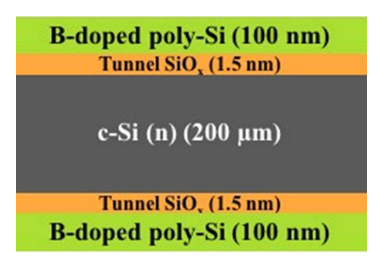


Fig. 1. Schematic diagram of p-TOPCon structure.

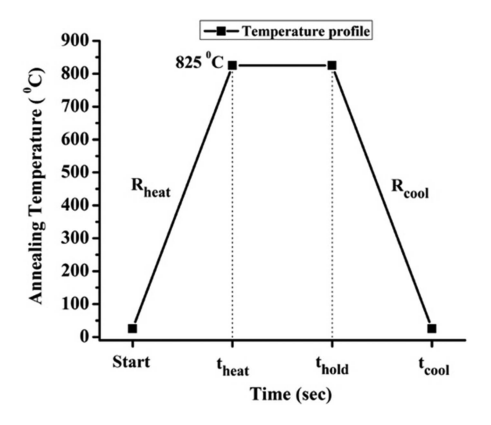


Fig. 2. Schematic diagram of the RTA temperature profile.

using piranha solution and SC-2, with oxide removal (5% wt. H.F. solution) between steps. A thin ( $\sim$ 1.5 nm) SiO<sub>x</sub> layer was grown on both sides of the Si using 70% wt. electronics grade HNO<sub>3</sub> at 100 °C for 15 min. Subsequently, *in situ* boron-doped polysilicon of 100 nm thickness was grown on both sides in a Tystar tube low-pressure chemical vapor deposition system at 588 °C for 27 min using silane and diborane precursor gases. A specific sample was annealed in nitrogen at 875 °C for 30 min in a Centrotherm tube furnace to enhance crystallinity and activate dopants.

Both RTA and forming gas anneals (FGAs) were conducted using the AnnealSys rapid thermal processing system, employing diverse processing gas environments, such as ultrapure N<sub>2</sub> and forming gas (5% H2: 95% Ar) from Praxair. The ambient humidity was approximately 40%. RTAs included heating from room temperature, holding at 825 °C and cooling in an N2 atmosphere [9]. Variations were made in heating time (30–150 s), holding time (10-150 s), and cooling time (30-300 s). The temperature profile of the RTA process is depicted in Fig. 2. An example of actual RTA temperature and power profile for heating, holding, and cooling times of 150 s, 150 s, and 600 s, respectively, is illustrated in Fig. 3. An average overshoot of  $\pm 25$ °C temperature was observed during the RTA heating time. The pyrometer works well at temperatures above 250 °C. In the first  $\sim$ 600 s, there was no temperature rise. For reference, p-TOPCon samples underwent annealing in a tube furnace at 875 °C for 30 min in N<sub>2</sub>, with a ramp-up from 600 °C at approximately 10 K/min. The FGA process comprised of annealing at 425 °C in forming gas for 1 h.

As shown in Fig. 4, the pulsed form of RTA was used to study the passivation quality under a series of pulsing heating,

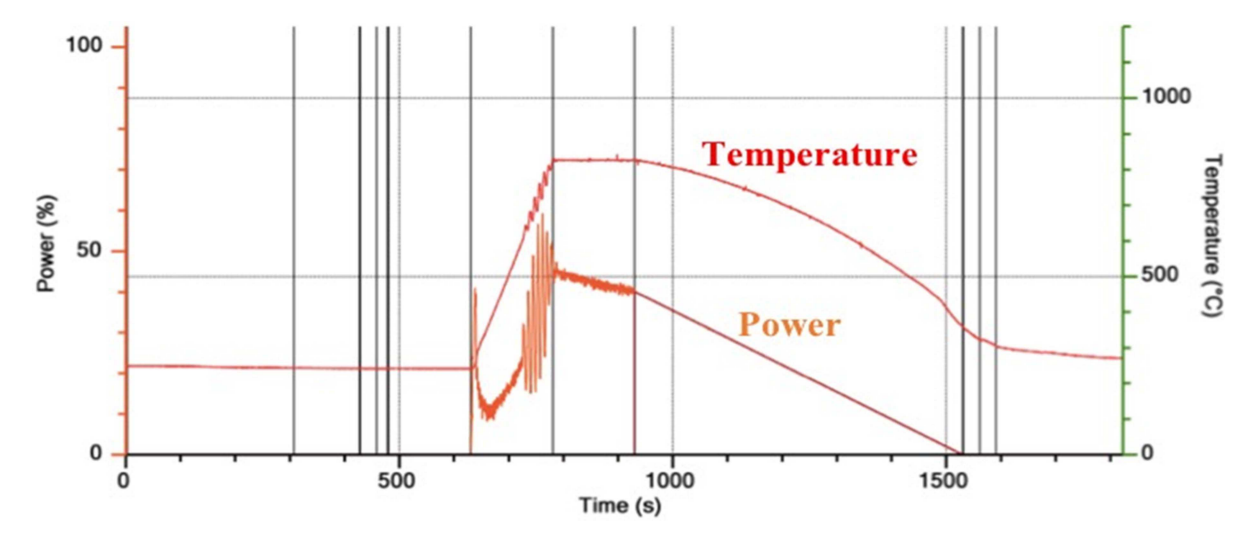


Fig. 3. Actual RTA temperature and lamp-power profile of annealing conditions at heating and holding times of 150 s each and a cooling time of 600 s.

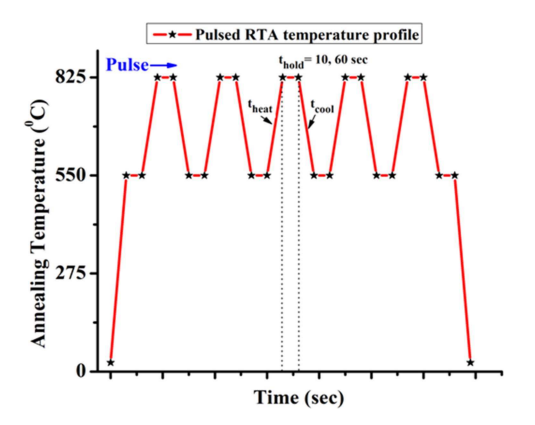


Fig. 4. Schematic diagram of the five pulses RTA temperature profile.

holding, and cooling times. Only  $t_{\rm hold}$  was varied as 10 s or 60 s. All other time frames, including time between any two pulses at 550 °C, consisted of 60 s. Such a design was formulated to relieve thermal stress.

Initial samples were extracted from a 6-in test wafer cut to a 1 cm  $\times$  1 cm area before further processing. QSSPC minority carrier lifetime and  $iV_{\rm oc}$  measurements were conducted using  $1''\times 1''$  area test samples on a WCT-120 Sinton Instruments system with a 4 cm diameter QSSPC sensor coil. Three samples were prepared for each thermal annealing test, with a film thickness variation of  $\pm 5\%$  within 1 cm length. Boron concentration homogeneity was not measured. For sheet resistance measurements, a Jandel four-point probe station was utilized.

The PL measurement is a nondestructive technique, and the intensity is related to the radiative carrier recombination. Higher PL intensity implies higher radiative recombination and less nonradiative recombination due to defects. So, higher PL intensity is related to higher junction quality. All PL measurements employed a 532 nm excitation wavelength with a  $\sim\!150~\mu m$  focused spot size. The peak PL intensity counts were determined at a wavelength of 1150 nm ( $\sim 1.1~eV$  Si bandgap) at an average of ten readings. The error bar for PL was measured to be 6%.

To investigate the effect of the B-doped poly-Si layer on the passivation quality and the extent of the boron dopant diffusion at the  ${\rm SiO_x/Si}$  interfaces, four test samples of 1 cm  $\times$  1 cm area, including the starting and the reference furnace anneal samples, were selected. The B-doped poly-Si layer was selectively etched using 20% wt. KOH at 40 °C for 250 s at an etch rate of -0.4 nm/s. Sample 1 was as-prepared (starting), sample 2 was furnace annealed, the third sample was KOH etched, and the fourth sample went through RTA and then KOH etched. The KOH etching kept the  ${\rm SiO_x}$  layer on the silicon wafer.

# III. RESULTS AND DISCUSSION

# A. Effects of Heating Time $T_{heat}$

Fig. 5(a) shows the variation of peak PL intensity and the sheet resistances w.r.t. the RTA heating time  $t_{\rm heat}$  at constant  $t_{\rm hold}=300~{\rm s}$  and  $t_{\rm cool}=300~{\rm s}$ . At  $t_{\rm heat}=10~{\rm s}$  or heating rate  $R_{\rm heat}=4800~{\rm K/min}$ , the peak PL intensity dropped from 450 to 110 a.u. As the time  $t_{\rm heat}$  was increased from 60 to 300 s (or  $R_{\rm heat}\leq780~{\rm K/min}$ ), the peak PL intensity climbed back and saturated at the PL intensity of the starting sample. The FGA recovered the peak PL intensity of test samples treated only at  $t_{\rm heat}\geq60~{\rm s}$  to a saturated value of  $\sim1525~{\rm a.u.}$  comparable with the furnace-annealed reference sample ( $\sim2100~{\rm a.u.}$ ), and the fast heated  $t_{\rm heat}=10~{\rm s}$  sample did not recover. This showed that a fast heating rate ( $R_{\rm heat}=4800~{\rm K/min}$ ) irreversibly degraded the surface passivation quality beyond recovery, and FGA could not improve it further. The optimized value of  $t_{\rm heat}$  is  $\geq60~{\rm s}$ .

The sheet resistance dropped significantly and saturated at 0.9–1.1 k $\Omega$ /sq. at fast heating rate  $R_{\rm heat} = 4800$  K/min, comparable with furnace anneal. The dip at  $t_{\rm heat} = 10$  s should be treated as within the error bar. This proved that a fast heating rate of 4800 K/min generates significant dopant activation.

# B. Effects of Holding Time $T_{hold}$

Fig. 5(b) shows the variation of peak PL intensity and the sheet resistances w.r.t. the RTA holding time  $t_{hold}$  at constant  $t_{heat}$  =

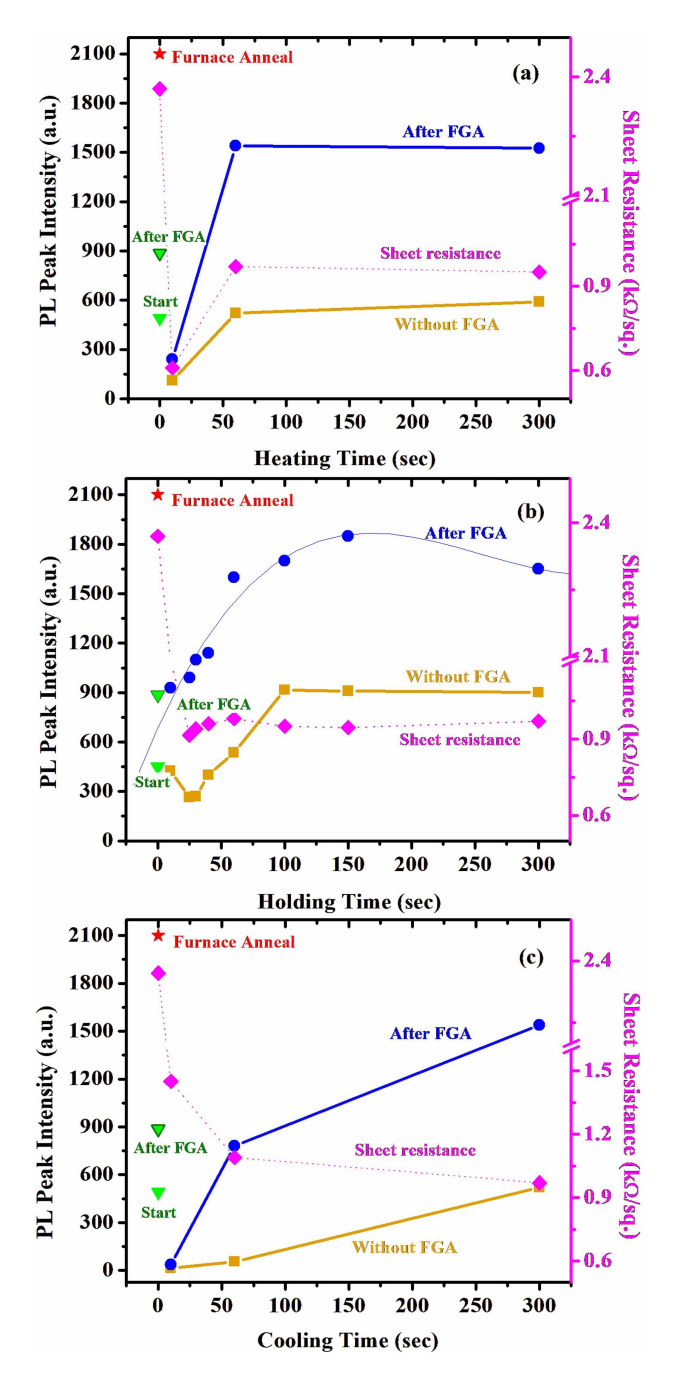


Fig. 5. Schematics of the dependence of peak PL intensity counts and sheet resistance on RTA (a) heating, (b) holding, and (c) cooling times. The data for as-prepared (start), after FGA treatment only, and furnace annealed are also shown

60 s and  $t_{\rm cool} = 300$  s. From  $t_{\rm hold} = 10$  s to 100 s, the peak PL intensity showed an increasing trend w.r.t. the starting condition. At  $t_{\rm hold} > 100$  s, PL intensity counts saturate. After FGA, both test samples under  $t_{\rm hold} = 60$  s and 300 s showed a significant jump in the peak PL intensity and saturated at  $\sim 1800$  a.u. The test sample with the shortest hold time of 10 s did not recover the PL intensity. This showed that a short holding time of 10 s caused irreversible degradation to the surface passivation quality beyond recovery, and FGA could not improve it further. The optimized condition for the value of  $t_{\rm hold}$  starts from 60 s.

TABLE I CARRIER LIFETIME,  $iV_{\rm OC}$ , AND SHEET RESISTANCE AFTER OPTIMIZED RTA

No.	RTA condition (s) at 825°C/N <sub>2</sub>		τ (μs)	iV <sub>OC</sub> (mV)	Sheet resistance (kΩ/sq.)	
1	-	Furnace Anneal	300	688	0.9-1.1	
	$t_{\text{heat}} = 60;$ $t_{\text{hold}} = 100;$ $t_{\text{cool}} = 300$	Starting	15	573		
2		After RTA	56	602	1.0-1.1	
		After FGA	97	628		
3	$t_{\rm heat} = 60;$ $t_{\rm hold} = 150;$ $t_{\rm cool} = 600$	Starting	11	571		
		After RTA	78	607	0.9-1.0	
		After FGA	112	633		
	$t_{\text{heat}} = 150;$ $t_{\text{hold}} = 150;$ $t_{\text{cool}} = 600$	Starting	14	571		
4		After RTA	72	609	0.9-1.0	
		After FGA	133	638		

The sheet resistance dropped significantly and saturated at 0.9–1.1 k $\Omega$ /sq. starting at a short holding time of 10 s, comparable with furnace anneal. Hence, dopant activation occurs at 10 s or longer hold time.

# C. Effects of Cooling Time $T_{cool}$

Fig. 5(c) shows the variation of peak PL intensity and the sheet resistances w.r.t. the RTA cooling time  $t_{cool}$  at constant  $t_{\rm heat} = 60 \text{ s}$  and  $t_{\rm hold} = 300 \text{ s}$ . At  $t_{\rm cool} = 10 \text{ s}$  or cooling rate  $R_{\rm cool} = 4800$  K/min, the peak PL intensity dropped from 450 to 12 a.u. As the time regime of  $t_{cool}$  was increased from 60 to 300 s (or  $R_{\rm cool} \leq 156$  K/min), the peak PL intensity climbed back gradually to the starting sample PL intensity counts. The peak PL intensity of the test sample treated under the shortest cooling time  $t_{cool} = 10$  s did not recover after FGA. On the other hand, the FGA regained the peak PL intensity of test samples treated at  $t_{\rm cool} = 60$  s to a value of  $\sim 800$  a.u., and the highest peak PL intensity rise to 1550 a.u. was recorded at  $t_{\rm cool} =$ 300 s comparable to furnace-annealed reference sample ( $\sim$ 2100 a.u.). It was observed that a fast quenching/cooling rate ( $R_{cool}$ = 4800 K/min) irreversibly degraded the surface passivation quality beyond recovery, and FGA could not improve it further. The optimized value of  $t_{\text{cool}}$  is  $\geq 300 \text{ s}$ .

Sheet resistances decreased gradually as the cooling rate fell, which showed that the dopant activation was affected moderately with a fast cooling rate.

# D. Optimization of RTA Parameters

For better device performance, the optimized RTA heating, holding, and cooling times were 60, 60, and 300 s. Table I presents some of the optimized performances of p-TOPCon devices after RTA.

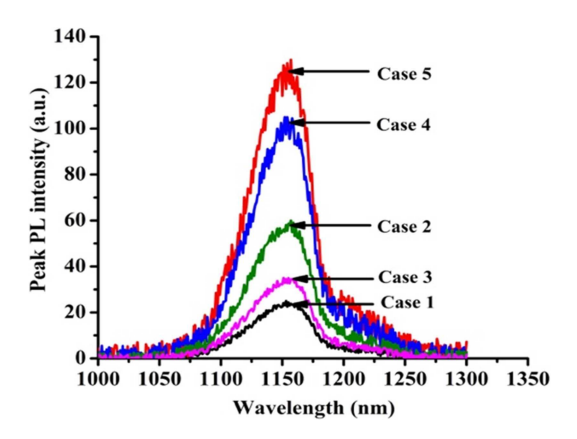


Fig. 6. Dependence of PL intensity counts for five cases described in Table II.

Table I also presents that the reference furnace anneal sample had sheet resistance of 0.9–1.0 k $\Omega$ /sq., a lifetime of  $\sim\!300~\mu s$ , and  $iV_{\rm oc}$  of 688 mV. Postanneal FGA further enhanced the overall performances. The sheet resistances were reduced to  $\sim\!0.9~{\rm k}\Omega/{\rm sq}$ , which showed that complete dopant activation was achievable under RTA conditions. However, the best performance of the RTA-annealed p-TOPCon device lagged behind the furnace-annealed device by  $\sim\!50~{\rm mV}$ . Using longer RTA durations may probably increase the  $iV_{\rm oc}$  and lifetime, but it will defeat the purpose of "rapidity" of our RTA processing.

The results of this study show that the  $iV_{\rm oc}$  of RTA p-TOPCon falls short compared with the furnace annealing. The RTA provides flexibility but the throughput of p-TOPCon is limited.

# E. Effect of B-Doped Poly-Si on Passivation Quality

Fig. 6 shows the dependence of PL intensity counts on the presence of boron-doped poly-Si layer. The test samples were treated under the RTA conditions  $t_{\rm heat} = 60~{\rm s}$ ,  $t_{\rm hold} = 100~{\rm s}$ , and  $t_{\rm cool} = 300~{\rm s}$  at 825 °C in N<sub>2</sub>. To evaluate the effect of boron diffusion into Si during the furnace and RTA annealing process, the doped poly-Si layer was chemically etched away after annealing, and the PL was measured. These results were compared with the samples that did not have doped poly-Si but went through RTA and furnace annealing under similar conditions.

The peak PL intensity counts derived from Fig. 6 have been tabulated in Table II. Comparing Case 1 with Case 2, it is observed that the RTA enhanced the passivation quality of the ultrathin  $\mathrm{SiO}_{\mathrm{x}}$  layer. Comparing Cases 1 and 3, it is observed that the presence of poly-Si layer provides additional passivation in the absence of RTA. In Case 4, it is observed that the RTA moderately improved the overall passivation quality. Case 5 shows the best passivation quality after furnace annealing.

In the case of RTA with a poly-Si layer, the boron dopants could diffuse through the pinholes in the  ${\rm SiO_x}$  layer into bulk Si. This diffused layer will provide additional field-effect passivation, exhibiting higher PL counts even after removing the poly-Si layer. The furnace-annealed samples showed the best performance due to the slower boron diffusion in bulk Si under a longer duration of heating and cooling times. In the case

TABLE II PEAK PL INTENSITY OF THE EFFECTS OF B-DOPED POLY-SI ON THE PASSIVATION QUALITY

Case	RTA at 825 °C $t_{\text{heat}} = 60 \text{ s}, t_{\text{hold}} = 100 \text{ s}, t_{\text{cool}} = 300 \text{ s}$	Peak PL Intensity (a.u.)
1	After SiO <sub>x</sub> deposition on Si	25
2	After the RTA of SiO <sub>x</sub> deposited on Si	57
3	After poly-Si deposition on SiO <sub>x</sub> /Si	33
4	After RTA of poly-Si deposition followed by its chemical etch	108
5	After Furnace anneal of poly-Si deposition followed by its chemical etch	127

TABLE III  ${\it IV}_{\rm OG}$  and Sheet Resistance After Optimized Pulsed RTA

Pulsed RTA Holding time (sec)	Number of RTA pulses	Starting sample peak PL intensity counts (a.u.)	After RTA peak PL intensity counts (a.u.)	After FGA peak PL intensity counts (a.u.)	Sheet resistance (kΩ/sq.)
	1	410	120	330	1.9
10	5		380	1200	1.45
	10		410	1350	1.35
	1		100	570	1.8
60	5		450	660	1.6
	10		390	1100	1.4

Both heating and cooling times were fixed at 60 s.

of RTA with a poly-Si layer, overdiffusion of boron might have caused Auger recombination, which lowered the passivation quality. This might also explain the cause of the discrepancy in the  $iV_{\rm oc}$  between optimized RTA and reference furnace anneal samples. The performance lag of p-TOPCon compared with the n-TOPCon could possibly be due to lower improvements in interface properties and the amount of boron diffusion in Si. It has been reported that boron diffusion is much faster under RTA compared with slow furnace annealing [22].

### F. Effects of Pulsed RTA Processing

This study aimed to investigate the effects of a series of short pulses of RTA on the dopant activation and passivation quality of p-TOPCon devices. The results have been tabulated in Table III.

At both holding times (10 and 60 s), the number of pulses varied from 1 to 10. There was a preliminary decrease in PL intensity after RTA for each holding time, which improved after multiple pulses. This confirmed that as the cumulative holding

times increased, the PL intensity counts increased, and the passivation quality improved, reaching back to the starting sample condition. A trend in PL intensity counts was observed with the increase in the number of pulses, which improved postanneal FGA. It is to be noted that the cooling time of each of the RTA pulses is the most influential aspect, as it eradicates any sort of defects formed during the heating and holding times of each RTA pulse. If we compare the results based on different holding times, the changes in PL intensity counts were similar within the error bar and suggested no significant difference in the final PL intensity counts.

In the case of sheet resistance measurements, a gradual decrease was observed with the increase in the number of RTA pulses. This suggested that the first RTA pulse started the dopant activations process, and the sheet resistance decreased from 2.4 to 1.9 k $\Omega$ /sq. Later, this trend saturated as the number of pulses increased. It is possible to lower the sheet resistance further by increasing the cumulative holding time and the number of RTA pulses, but it will defeat the purpose of "rapidity" in our RTA processing. Our results show that the RTA process for p-TOPCon does not improve the  $iV_{\rm oc}$  at the same level as furnace annealing and for n-TOPCon. This possibly could be due to higher boron diffusion under the RTA process.

### IV. CONCLUSION

A scientific study was conducted to investigate the effects of heating, holding, and cooling time on the passivation quality and dopant activations during RTA processing (at 825 °C/N<sub>2</sub>) of in situ boron-doped p-TOPCon solar cells. Fast heating and cooling rates ( $\geq 4800 \text{ K/min}$ ) damaged the passivation quality irreversibly, beyond any postanneal FGA recovery. Slower heating (< 780 K/min) and cooling (< 156 K/min) rates provided the best PL intensity results. The start of the dopant activation process required at least 10 s of holding time, which was determined by the decreasing trend in the sheet resistance. The RTA parameters were optimized at a heating time of 60 s, a holding time of 60 s, and a cooling time of 300 s. At optimized parameters, considerable improvements in peak PL intensity counts and passivation quality of the test devices were observed, which further improved with the external FGA hydrogenation. The best performances were recorded as carrier lifetime of 133  $\mu$ s,  $iV_{oc}$ of 638 mV, and sheet resistance of  $\sim$ 0.9 k $\Omega$ /sq. at a heating time of 150 s, a holding time of 150 s, and a cooling time of 600 s. The RTA processing of etched poly-Si proved that the boron dopant diffusion could provide additional field-effect passivation. An overdiffused dopant profile creates Auger recombination and is detrimental to the overall passivation quality. The pulsed RTA processing showed the potential to adequately create dopant activation and passivation, and longer cumulative holding times can give better results.

Based on the study of RTA of p-TOPCon Photovoltaic (PV) devices, the following observations are made.

1) The  $iV_{\rm OC}$  results of RTA n-TOPCon are comparable to furnace annealing [8]. However, our results show that  $iV_{\rm OC}$  for RTA of p-TOPCon is lower than furnace annealing.

- The RTA of p-TOPCon sheet resistance is similar to furnace annealing.
- 3) The mechanism of the cooling rate effects on  $iV_{\rm OC}$  needs to be further investigated so that shorter RTA duration can be achieved. Further research is required to improve the performance of p-TOPCon devices under short RTA conditions in order to achieve high throughput.
- 4) The RTA of poly-Si/SiO<sub>x</sub>/c-Si improves the SiO<sub>x</sub>/c-Si interface quality and may induce boron diffusion to the interface, as evidenced by the observation of higher PL intensity after the poly-Si removal.
- 5) The RTA studies show that the heating and the hold time can be in minutes. This information could be applied to furnace annealing conditions to lower the thermal budget and total annealing duration further.

### REFERENCES

- [1] A. Richter et al., "n-type Si solar cells with passivating electron contact: Identifying sources for efficiency limitations by wafer thickness and resistivity variation," Sol. Energy Mater. Sol. Cells, vol. 173, pp. 96–105, Dec. 2017, doi: 10.1016/j.solmat.2017.05.042.
- [2] F. Haase et al., "Laser contact openings for local poly-Si-metal contacts enabling 26.1%-efficient POLO-IBC solar cells," Sol. Energy Mater. Sol. Cells, vol. 186, pp. 184–193, 2018, doi: 10.1016/j.solmat.2018.06.020.
- [3] L. Nasebandt et al., "Sputtered phosphorus-doped poly-Si on oxide contacts for screen-printed Si solar cells," Sol. RRL, vol. 6, no. 9, Sep. 2022, Art. no. 2200409, doi: 10.1002/solr.202200409.
- [4] S. Choi et al., "Formation and suppression of hydrogen blisters in tunnelling oxide passivating contact for crystalline silicon solar cells," Sci. Rep., vol. 10, no. 1, Jun. 2020, Art. no. 9672, doi: 10.1038/s41598-020-66801-4.
- [5] Z. Zhang et al., "Improvement of surface passivation of tunnel oxide passivated contact structure by thermal annealing in mixture of water vapor and nitrogen environment," Sol. RRL, vol. 3, no. 10, Oct. 2019, Art. no. 1900105, doi: 10.1002/solr.201900105.
- [6] G. C. Wilkes, A. D. Upadhyaya, A. Rohatgi, and M. C. Gupta, "Laser crystallization and dopant activation of a-Si:H carrier-selective layer in TOPCon Si solar cells," *IEEE J. Photovolt.*, vol. 10, no. 5, pp. 1283–1289, Sep. 2020, doi: 10.1109/JPHOTOV.2020.3006273.
- [7] D. K. Ghosh et al., "Fundamentals, present status and future perspective of TOPCon solar cells: A comprehensive review," *Surfaces Interfaces*, vol. 30, Jun. 2022, Art. no. 101917, doi: 10.1016/j.surfin.2022.101917.
- [8] Q. Yang et al., "In-situ phosphorus-doped polysilicon prepared using rapid-thermal anneal (RTA) and its application for polysilicon passivatedcontact solar cells," Sol. Energy Mater. Sol. Cells, vol. 210, Jun. 2020, Art. no. 110518, doi: 10.1016/j.solmat.2020.110518.
- [9] A. Sinha, S. Dasgupta, A. Rohatgi, and M. C. Gupta, "Rapid thermal annealing of p-type polysilicon passivated contacts silicon solar cells," *IEEE J. Photovolt.*, vol. 13, no. 3, pp. 355–364, May 2023, doi: 10.1109/JPHOTOV.2023.3241790.
- [10] L. P. Welsh, J. A. Tuchman, and I. P. Herman, "The importance of thermal stresses and strains induced in laser processing with focused Gaussian beams," *J. Appl. Phys.*, vol. 64, no. 11, pp. 6274–6286, Dec. 1988, doi: 10.1063/1.342086.
- [11] G. Yang et al., "Will SiO -pinholes for SiO /poly-Si passivating contact enhance the passivation quality?," Sol. Energy Mater. Sol. Cells, vol. 252, Apr. 2023, Art. no. 112200, doi: 10.1016/j.solmat.2023.112200.
- [12] A. S. Kale et al., "Effect of silicon oxide thickness on polysilicon based passivated contacts for high-efficiency crystalline silicon solar cells," Sol. Energy Mater. Sol. Cells, vol. 185, pp. 270–276, Oct. 2018, doi: 10.1016/j.solmat.2018.05.011.
- [13] Z. Yang et al., "Charge-carrier dynamics for silicon oxide tunneling junctions mediated by local pinholes," *Cell Rep. Phys. Sci.*, vol. 2, no. 12, Dec. 2021, Art. no. 100667, doi: 10.1016/j.xcrp.2021.100667.
- [14] C. Hollemann, F. Haase, J. Krugener, R. Brendel, and R. Peibst, "Firing stability of n-type poly-Si on oxide junctions formed by quartz tube annealing," in *Proc. 47th IEEE Photovolt. Specialists Conf.*, 2020, pp. 1274–1278, doi: 10.1109/PVSC45281.2020.9300849.

- [15] C. Hollemann et al., "Changes in hydrogen concentration and defect state density at the poly-Si/SiOx/c-Si interface due to firing," Sol. Energy Mater. Sol. Cells, vol. 231, Oct. 2021, Art. no. 111297, doi: 10.1016/j.solmat.2021.111297.
- [16] S. M. Hu, "Stress-related problems in silicon technology," J. Appl. Phys., vol. 70, no. 6, pp. R53–R80, Sep. 1991, doi: 10.1063/1.349282.
- [17] A. Rohatgi, Z. Chen, P. Doshi, T. Pham, and D. Ruby, "High-efficiency silicon solar cells by rapid thermal processing," *Appl. Phys. Lett.*, vol. 65, no. 16, pp. 2087–2089, Oct. 1994, doi: 10.1063/1.112801.
- [18] P. Doshi et al., "Rapid thermal processing of high-efficiency silicon solar cells with controlled in-situ annealing," Sol. Energy Mater. Sol. Cells, vol. 41–42, pp. 31–39, Jun. 1996, doi: 10.1016/0927-0248(95)00119-0.
- [19] C. Sen et al., "Assessing the impact of thermal profiles on the elimination of light- and elevated-temperature-induced degradation," *IEEE J. Photovolt.*, vol. 9, no. 1, pp. 40–48, Jan. 2019, doi: 10.1109/JPHOTOV.2018.2874769.

- [20] H. A. Lord, "Thermal and stress analysis of semiconductor wafers in a rapid thermal processing oven," *IEEE Trans. Semicond. Manuf.*, vol. 1, no. 3, pp. 105–114, Aug. 1988, doi: 10.1109/66.4383.
- [21] C. Shou et al., "Optimization of tunnel-junction for perovskite/tunnel oxide passivated contact (TOPCon) tandem solar cells," *Physica Status Solidi*, vol. 218, no. 24, Dec. 2021, Art. no. 2100562, doi: 10.1002/pssa.202100562.
- [22] S. Guimarães, E. Landi, and S. Solmi, "Enhanced diffusion phenomena during rapid thermal annealing of preamorphized boron-implanted silicon," *Physica Status Solidi*, vol. 95, no. 2, pp. 589–598, Jun. 1986, doi: 10.1002/pssa.2210950228.